Synthesis and characterization of graphene related nanomaterials by catalytic decomposition of methane using transition metal catalysts

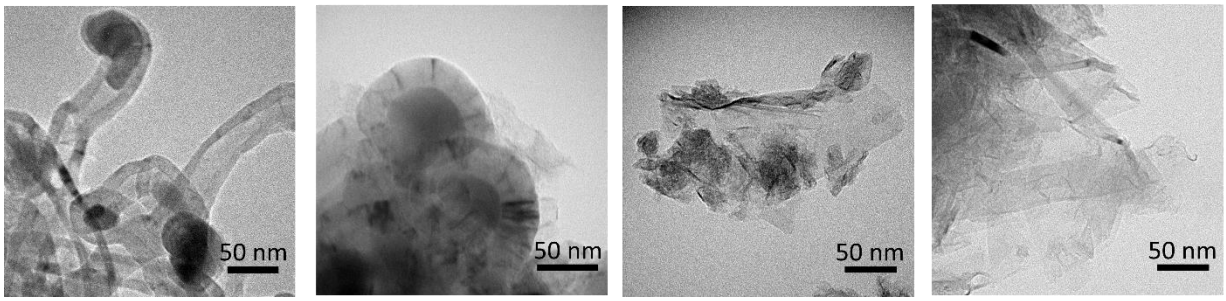

Wilson Albeiro Henao Sierra

Final Master Project

Master's degree in Nanostructured Materials for Nanotechnology Applications

Tutored by

Dr. Antonio Monzón Bescós

Dr. Eva María Romero Salazar

CREG-Catalysis, Molecular Separations & Reactor Engineering Group

28th June 2019, Zaragoza-Spain

“Hay hombres que luchan un día y son buenos.
Hay otros que luchan un año y son mejores.
Hay quienes luchan muchos años, y son muy buenos.
Pero hay los que luchan toda la vida:
esos son los imprescindibles”

Bertolt Brecht

*"Un hombre del pueblo de Neguá, en la costa de **Colombia**, pudo subir al alto cielo.*
A la vuelta contó. Dijo que había contemplado desde arriba, la vida humana.
Y dijo que somos un mar de fueguitos.
-El mundo es eso -reveló- un montón de gente, un mar de fueguitos.
Cada persona brilla con luz propia entre todas las demás.
No hay dos fuegos iguales.
Hay fuegos grandes y fuegos chicos y fuegos de todos los colores.
Hay gente de fuego sereno, que ni se entera del viento,
y gente de fuego loco que llena el aire de chispas.
Algunos fuegos, fuegos bobos, no alumbran ni queman;
pero otros arden la vida con tanta pasión
que no se puede mirarlos sin parpadear,
y quien se acerca se enciende"

Eduardo Galeano

Abstract

This work presents the selective synthesis of graphene-related nanomaterials and carbon nanotubes via catalytic decomposition of methane using carbon catalysts derived from cellulose (CDC) and impregnated with Co, Mn or Cu transition metals. The catalysts were prepared by reductive thermal decomposition of a commercial cellulose previously impregnated with the metallic precursors. The incorporation of Mn or Cu as metal promotors was found to direct the reaction towards the formation of a desired carbonaceous nanomaterial (CNM). Co-Mn/CDC catalyst was selective towards the production of graphene-related nanomaterials (few-layer graphene (FLG), graphite nanolayers and graphene nanoflakes) at reaction temperatures above 900 °C, whereas Co-Cu/CDC catalyst favored the formation of carbon nanotubes at temperatures below 850 °C. The influence of the operating conditions —reaction temperature and feed gas composition (%CH_4:%H_2)— on the quality and productivity of the obtained CNMs was evaluated by Raman spectroscopy and electron microscopy. The productivity and growth rate of CNMs were favored by increasing both the temperature and methane percentage on the feed. The maximum productivity reached by the Co-Mn/CDC catalyst was 0.48 gC/gcat·h at 975 °C with a feed composition of 28.6%CH_4:14.3%H_2:57.1%N_2. On the other hand, in the Co-Cu/CDC catalyst this productivity was 0.38 gC/gcat·h at 750 °C using a feed composition of 42.9%CH_4:14.3%H_2:42.9%N_2. The carbon growth evolution was further analyzed by a phenomenological kinetic model developed in previous works by the Dr. Antonio Monzon research team at the CREG-Catalysis, Molecular Separations & Reactor Engineering Group.

Keywords: Carbon nanotubes, graphene related materials, methane decomposition, transition metals

Contents

1. Introduction

During the last years, the production of carbonaceous nanomaterials (CNMs), such as nanotubes (CNTs), nanofibers (CNFs) and graphene-related materials (few-layer graphene (FLG), graphite nanolayers, graphene nanoflakes) has received a great industrial and scientific interest due to their extraordinary physical and chemical properties [1]. Nowadays, enormous efforts are being devoted to finding the optimal operating conditions and the most suitable catalysts that provide high carbon yield, quality and selectivity towards a desired CNM for large-scale production processes. Among the current available technologies to produce these fascinating nanomaterials, the catalytic chemical vapor decomposition (CCVD) of hydrocarbons emerges as an attractive method for meeting this demand, due to its low-cost and easy scalability for mass production [2].

In this technique, transition metal catalyst nanoparticles are exposed to a gaseous carbon precursor, commonly a light hydrocarbon (e.g., CH_4, C_2H_2, C_2H_4), at elevated temperatures (600–1200º C), which is decomposed into carbon atoms that diffuse and precipitate through the metal nanoparticles to form the carbonaceous nanomaterial. The growth of the carbonaceous material continues as long as the metallic nanoparticles have active sites available for the hydrocarbon cracking and there is a favorable carbon concentration difference between the surface of the nanoparticle exposed to the gas and the exit points where precipitation and segregation of the carbon atoms occur [3].

Most commonly used transition metals are Fe, Co, Ni, because of their high carbon solubility and carbon diffusion rate at high temperatures. Nevertheless, other metals such as Cu, Pt, Pd, Mn, Mo, Cr, Sn, Au, Mg, Al has also been tested in the CNMs production by CCVD, since they allow modulate the carbon atoms diffusion and the final structure of the CNM obtained [4].

In order to improve the quality and production of the CNMs, the design of new catalyst formulations, of both the metal nanoparticles and the materials support, is being increasingly investigated. It is well-known that the support also plays an important role in the dispersion and catalytic activity of the metal, which in turn affects the properties of the CNMs formed [5,6]. The use of lignocellulosic agricultural wastes as catalytic supports for the CNMs production emerges as an attractive alternative to the conventional inorganic materials supports based on metal oxides, because their large availability and

unique textural properties can provide a fine dispersion of metal nanoparticles, and increase the number of nucleation sites which is advantageous to the high yield synthesis of CNMs [7].

In this work, the selective production of CNts and graphene-related nanomaterials is investigated via catalytic decomposition of methane (CDM) by using a Co/carbon catalyst derived from cellulose (CDC) modified with Cu or Mn. The influence of the operating conditions —reaction temperature and feed gas composition— on the quality and productivity of the obtained carbonaceous nanomaterials is evaluated.

Since the controllable large-scale production of CNMs with a desired structure requires a fundamental understanding of the growth mechanism and the synthesis condition process, in this work the effect of the operating conditions on the carbon growth evolution is further analyzed by using a phenomenological kinetic model developed in previous works by the Dr. Antonio Monzon research team at the CREG-Catalysis, Molecular Separations & Reactor Engineering Group [8-12]. This kinetic model considers the fundamental steps of the growth reaction mechanism of CNMs, involving the i) adsorption and catalytic decomposition of the gas carbon precursor on the metal nanoparticles surface; ii) formation of a metastable metallic carbide on the surface of the metal nanoparticles, which, under reaction conditions, decomposes leaving carbon atoms at the metallic subsurface; iii) diffusion of carbon atoms through the metal particle or along its surface and its subsequent precipitation at the metal-support interface; iv) formation and growth of carbonaceous nanomaterial; v) growth termination either by catalyst deactivation or by steric hindrance of the nanomaterial grown.

2. Materials and methods

2.1. Catalysts preparation

Co-(Cu or Mn)/CDC catalysts were prepared by reductive thermal decomposition of a commercial cellulose (Sigma Aldrich, ref: C6288) following the procedure described in [6]. First, the cellulose was dried at 100 °C overnight and then impregnated by incipient wetness with the appropriate amount of an aqueous solution containing the metal precursor salts ($Co(NO_3)_2 \cdot 6H_2O$, $Cu(NO_3)_2 \cdot 3H_2O$ or $Mn(NO_3)_2 \cdot 4H_2O$, Sigma-Aldrich). The nominal metal content in each catalyst was 5%Co-1.35%Cu/CDC and 3.5%Co-3.3%Mn/CDC with respect to the initial amount of cellulose. After impregnation, the solids were dried at 80 °C and thermally decomposed under a reductive atmosphere (15% H_2, 85% N_2, 400mL/min) at 900 °C for 180 min, with a heating rate of 50 °C/min. Finally, the catalysts were milled and sieved obtaining a particle size distribution ranging from 10 µm to 200 µm.

2.2. Catalytic decomposition of methane

Catalytic decomposition of methane (CDM) was carried out under atmospheric pressure in a quartz thermobalance (CI Electronics Ltd., UK, model MK2) operated as a continuous differential fixed-bed reactor.

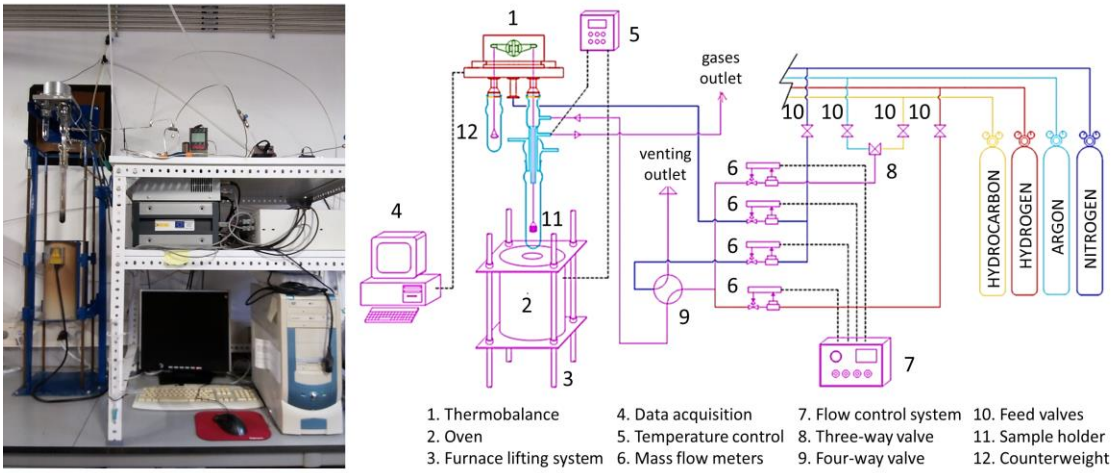

Fig. 1. Quartz thermobalance set up (CI Electronics Ltd., UK, model MK2). Modified from [13].

The carbon mass evolution and the temperature were continuously recorded during the growth of the carbonaceous nanomaterial along 120 min of reaction. The temperature range evaluated was 650–975 °C

while the feed composition was variated from 7.1% to 42.9% of CH_4 and H_2, using N_2 as balance gas (total flow rate 700 mL/min). In a typical experiment, ca. 25 mg catalyst were placed into a copper mesh sample holder and then, after performing a weight calibration procedure, the sample was heated at 10 ºC/min under a N_2 flow of 700 mL/min until reaching the reaction temperature. Once the selected reaction temperature was reached, the reactive gas mixture comprising $CH_4/H_2/N_2$ was introduced into the reactor keeping the temperature constant for 120 min. Finally, the sample was cooled down to room temperature under N_2 atmosphere.

2.3. Catalysts and carbonaceous nanomaterials characterization

The metal content of the cellulose-derived carbon (CDC) catalysts was determined by thermogravimetric analysis under oxidative atmosphere (air, 50 mL/min) in a Mettler Toledo TGA/SDTA 851 analyzer. Approximately 5−10 mg of sample was heated from room temperature to 1000 ºC with a heating rate of 10 ºC/min. The weight percentage of each metal was calculated considering the metal nominal amount incorporated during the impregnation and the solid residue obtained after the TGA-Air experiment. Upon combustion, the solid residue comprises a mixture of ashes and metal oxides (CoO/CuO and Co_3O_4/MnO for the Co-Cu/CDC and Co-Mn/CDC catalyst, respectively). The final percentage of each component was calculated by subtracting the initial amount of metals incorporated from that of the respective metal oxides.

Specific surface area and porosity were obtained from N_2 adsorption–desorption isotherms at -196 °C using a TriStar 3000 instrument. Prior to the analysis, the samples were degassed at 200 °C for 8 h. BET specific surface areas were measured in the relative pressure range of 0.01–0.10. The total pore volume was obtained at the maximum relative pressure reached by the adsorption branch (P/Po> 0.989), whereas the micropore volume was estimated by the t-plot method.

Crystalline phase identification of the metal particles after the catalysts synthesis was performed by x-ray diffraction (XRD) in a Rigaku D/Max 2500 apparatus from 5° to 90° 2θ degrees using Cu Kα radiation (λ = 1.5406 Å). Chemical surface composition was characterized by X-Ray photoelectron spectroscopy (XPS) in a Kratos Axis ULTRA spectrometer using non-monochromatized Al Kα radiation (hυ= 1486.7 eV). All the spectra were analyzed in the CASA® XPS software by applying a Shirley-type background.

The morphology of the carbonaceous nanomaterials formed during the CDM reaction was determined by electron microscopy. Transmission electron microscopy (TEM) micrograph images were recorded in a FEI Tecnai T-20 microscope, operated at 200 kV. Scanning electron microscopy (SEM) micrograph images were taken in a FEI Inspect F50 microscope, operated at 10 kV.

The carbonaceous nature of the catalyst support and the quality of the nanomaterials grown were characterized by Raman spectroscopy using a WiTec Alpha300 confocal Raman microscope, with a 488 nm laser excitation beam. Since Raman scattering is highly sensitive to the electronic structure of the carbon nanomaterials, the intensity ratio between the characteristic D, G and 2D bands (I_G/I_D, I_{2D}/I_G) of an average of 5 spectra from different sample spots, were used to evaluate the amount of defects in the sp^2-hybridized carbon structures. In this work, the quantification of the disorder degree was addressed by measuring intensity ratios I_G/I_D , I_{2D}/I_G, instead of area ratio A_G/A_D , A_{2D}/A_G, due to the amorphous nature of the carbonaceous support [14].

2.4. Kinetic growth model

The growth kinetics of the synthesized carbonaceous nanomaterials was addressed by a phenomenological model developed in previous works by the CREG-Catalysis, Molecular Separations & Reactor Engineering Group [8-12].

This kinetic growth model considers the fundamental steps of the reaction mechanism summarized in **Scheme 1**, comprising the i) adsorption and catalytic decomposition of the methane molecules on the metal nanoparticles surface; ii) formation of a metastable metallic carbide on the surface of the metal nanoparticles, which, under reaction conditions, decomposes leaving carbon atoms at the metallic subsurface; iii) diffusion of carbon atoms through the metal particle, or along its surface, and subsequent precipitation at the metal-support interface; iv) formation and growth of carbonaceous nanomaterial whose nature (CNT, CNF, FLG) depends on the operating conditions and catalyst used; v) growth termination either due to catalyst deactivation or steric hindrance of the nanomaterial grown.

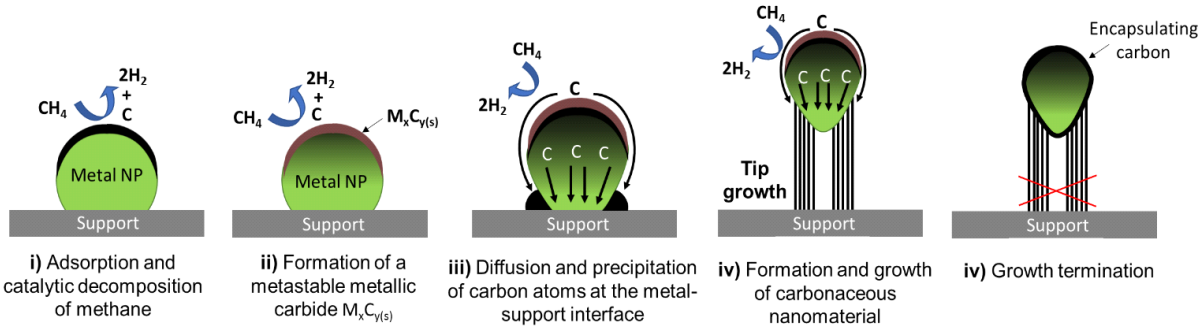

Scheme 1. Formation of carbonaceous nanomaterials by catalytic decomposition of methane.

Accordingly, the evolution of the carbon grown concentration m_C along the time (gC/gcat), was fitted by the following expression (furthermore information about the development and assumptions of the model is described in the **Annex I**):

$$m_C = j_{C_0} \cdot \left(a_R \cdot t^n + \frac{(1 - a_R)}{\psi_G} \cdot (1 - \exp(-\psi_G \cdot t^n)) \right) \qquad (1)$$

Where j_{C_0} represents the intrinsic carbon growth rate for the fresh catalyst, measured in gC/gcat·min, which depends on the effective carbon diffusivity through the metallic nanoparticles at the operating conditions. The term a_R corresponds to the residual activity of the catalyst, due to the partial regeneration of the catalyst surface by action of H_2 present in the reaction. The term ψ_G is defined as the sum $\psi_G = \psi_d + \psi_r$ of the kinetic parameters of deactivation and regeneration, respectively, and has dimensions of time^{-1}. Finally, n is a power parameter which allows modulating the effect of the diffusion time of carbon in each range of reaction temperature.

Since these parameters are dependent on the temperature and gas composition used in each experiment, the dependence with respect to the methane concentration can be expressed as power-law functions:

$$j_{C_0} = k_C \cdot P_{CH_4}^{m_C} \quad ; \quad \psi_d = k_d \cdot P_{CH_4}^{m_d} \quad ; \quad \psi_r = k_r \cdot P_{CH_4}^{m_r} \qquad (\mathbf{8})$$

The values of k_C, k_d, and k_r in the above equations follow an Arrhenius-type dependence with the temperature:

$$k_C = k_{C_0} \cdot \exp(-E_C/RT) \quad ; \quad k_d = k_{d_0} \cdot \exp(-E_d/RT) \quad ; \quad k_r = k_{r_0} \cdot \exp(-E_r/RT) \qquad (\mathbf{9})$$

Where E_C, E_d, and E_r represent the apparent activation energies for each parameter, and k_{C_0}, k_{d_0}, and k_{r_0} are the corresponding pre-exponential factors. These parameters were estimated by non-linear least-squares multivariable regression, using the Model Selection Criterion (MSC) as maximized objective function, defined as:

$$MSC = \ln\left(\frac{SST}{SSR}\right) - \left(\frac{2p}{n_p - p}\right) \quad (\mathbf{10})$$

In this expression, p represents the number of parameters and n_p the number of experimental points. The terms SST and SSR are the sum of total squares and the sum of the squared residuals, respectively:

$$SST = \sum_{i=1}^{i=n_p} \left(m_C^{exp} - \overline{m_C^{exp}}\right)^2 \quad ; \quad SSR = \sum_{i=1}^{i=n_p} \left(m_C^{exp} - m_C^{cal}\right)^2 \quad (\mathbf{11})$$

3. Results and Discussions

3.1. Fresh catalysts characterization

Co-Cu/CDC and Co-Mn/CDC catalysts were prepared with a nominal metal composition (wt.%) of 5%Co-1.35%Cu and 3.5%Co-3.3%Mn, respectively, regarding the initial amount of cellulose. After reductive thermal decomposition, the metal content (wt.%) of the catalysts determined by TGA-Air, were 23.9%Co-6.4%Cu for Co-Cu/CDC and 14.4%Co-13.4%Mn for Co-Mn/CDC, respecting to the final amount of biomorphic carbon formed. The increasing of the metal percentages in the resultant catalysts is due to the loss of carbonaceous material during the thermal decomposition stage. Nevertheless, the atomic ratios Co/Cu=4 and Co/Mn=1 were retained after catalysts preparation, which was corroborated by EDX spectroscopy.

The morphology of the prepared cellulose-derived carbon (CDC) catalysts was determined by electron microscopy shown in **Figure 1**. Both catalysts exhibited rough and irregular particles with a broad size distribution ranging from 10 to 200 μm. TEM images were used to estimate the particle size distribution of the incorporated metals by measuring at least 500 particles from different sample areas. Co-Mn/CDC exhibited a broad monomodal distribution of metal nanoparticles with an average size of 45 nm. On the other hand, Co-Cu/CDC presented a trimodal distribution with a high number of particles

around 3 nm and few particles with diameters around 11 nm and 21 nm. The broad metal nanoparticles size distribution observed in both catalysts is related to the high temperature and high heating rate used during the thermal decomposition stage of the materials synthesis.

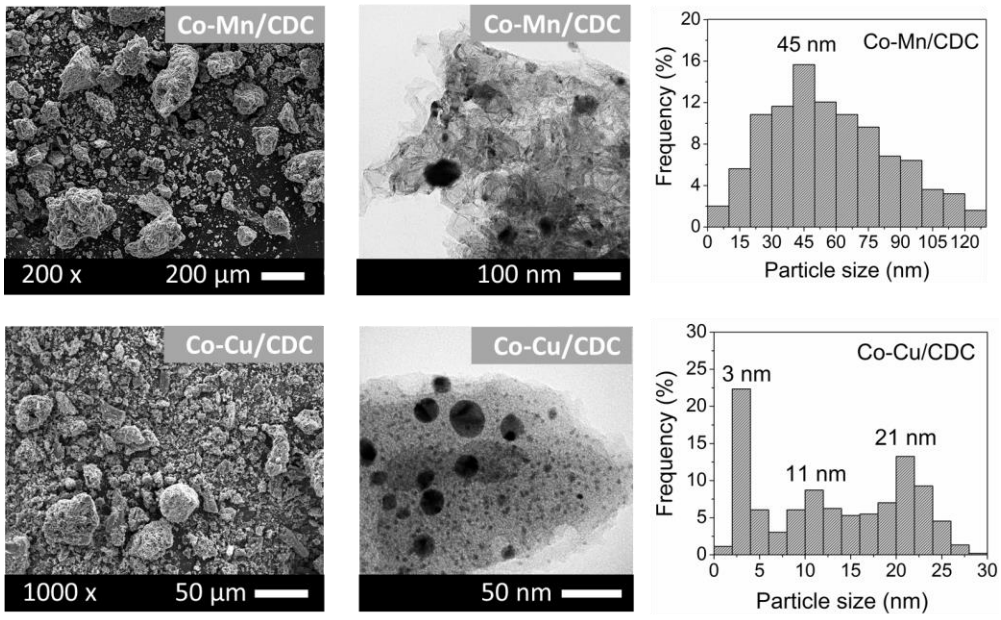

Figure 1. SEM and TEM images of the Co-Mn/CDC and Co-Cu/CDC fresh catalysts *(left)*, and their respective metal particle size distribution *(right)*.

Figure 2 shows the XRD pattern of the fresh catalysts before the catalytic methane decomposition reaction. In the Co-Cu/CDC pattern, it was observed that both Co and Cu were present in metallic state (Co^0, Cu^0), and no diffraction peaks ascribed to their respective metal oxides were identified. Conversely, in the Co-Mn/CDC catalyst, it was observed that Mn was mainly oxidized to MnO and the appearance of three additional peaks at ca. 41.2º, 47.9º and 70.2º 2θ degrees suggested the formation of a Co_2Mn_2C bimetallic carbide during the catalyst preparation. However, it is expected that during the CDM reaction, the H_2 present in the feed gas mixture (CH_4, H_2, N_2) promotes the reduction of such MnO particles to Mn^0, so that their catalytic activity is not compromised. The (002) reflection from the hexagonal graphite structure of the carbonaceous support was present in both catalyst patterns, being more defined in the case of Co-Mn/CDC.

Regarding the textural properties, the Co-Cu/CDC catalyst exhibited a surface area of 438 m^2/g, 0.194 cm^3/g pore volume, 87% microporosity and an average pore diameter of 0.77 nm. In case of Co-Mn/CDC, these values were 64 m^2/g, 0.117 cm^3/g, 26% and 11 nm, respectively. The decrease in the textural

properties of the Co-Mn/CDC catalyst can be attributed to the micropores blockage due to the presence of large nanoparticles as was observed in TEM images of **Figure 1**.

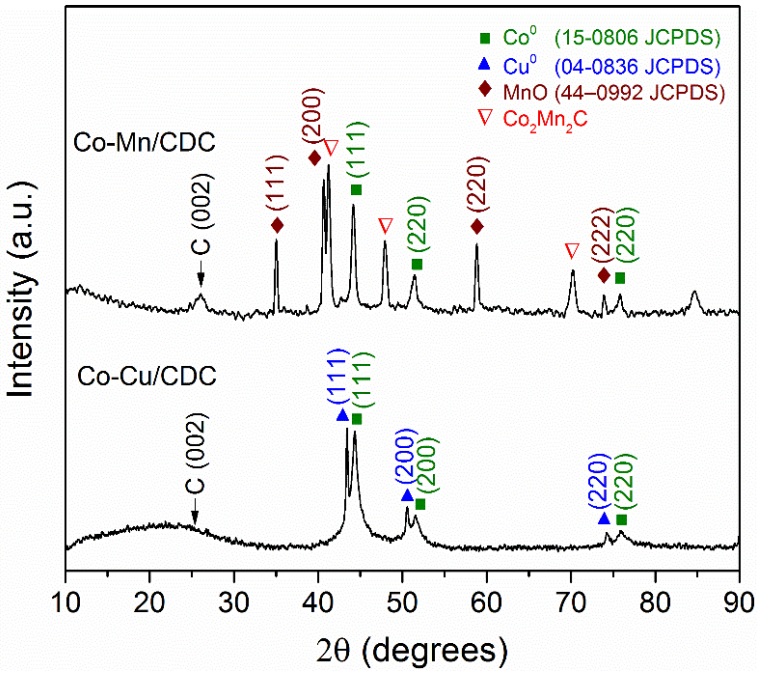

Figure 2. XRD diffraction pattern of the Co-Mn/CDC and Co-Cu/CDC fresh catalysts.

Figures 3A and **3B** show the Raman spectra of the fresh Co-Mn/CDC and Co-Cu/CDC catalysts, respectively. Both catalysts presented the characteristic high-intensity G (1584 cm^{-1}) and D (1348 cm^{-1}) bands of graphitic materials, which were attributed to the in-plane vibration of the C sp^2 bonds and the presence of C sp^3 defects within the carbonaceous network of the support, respectively [15]. Co-Mn/CDC exhibited a ratio I_G/I_D= 0.72 while in the Co-Cu/CDC this value was I_G/I_D= 1.04, suggesting that the Co-Mn/CDC contains a larger number of localized defects in its carbonaceous structure. Additionally, the spectra showed inset illustrate the Lorentzian fit deconvolution of the D and G bands into five peaks, which are related to several structural domain contributions [16]. These peaks were associated to the contribution of the C=C chain stretching and CH wagging modes (peak 1 at ca. 1250 cm^{-1}) [17], to the in-plane vibrations of the sp^2 bonded carbon within structural defects (peak 2 (D) at ca. 1350 cm^{-1}) [18,19], to the amorphous sp^2 carbon bonded phase (peak 3 at ca. 1490 cm^{-1}) [19], to the in-plane vibrations of the sp^2 bonded crystallite carbon (peak 4 (G) at ca. 1584 cm^{-1}) [20] and to the disorders resulting from the finite size effect or lattice distortion (peak 5 at ca. 1616 cm^{-1}) [20,21].

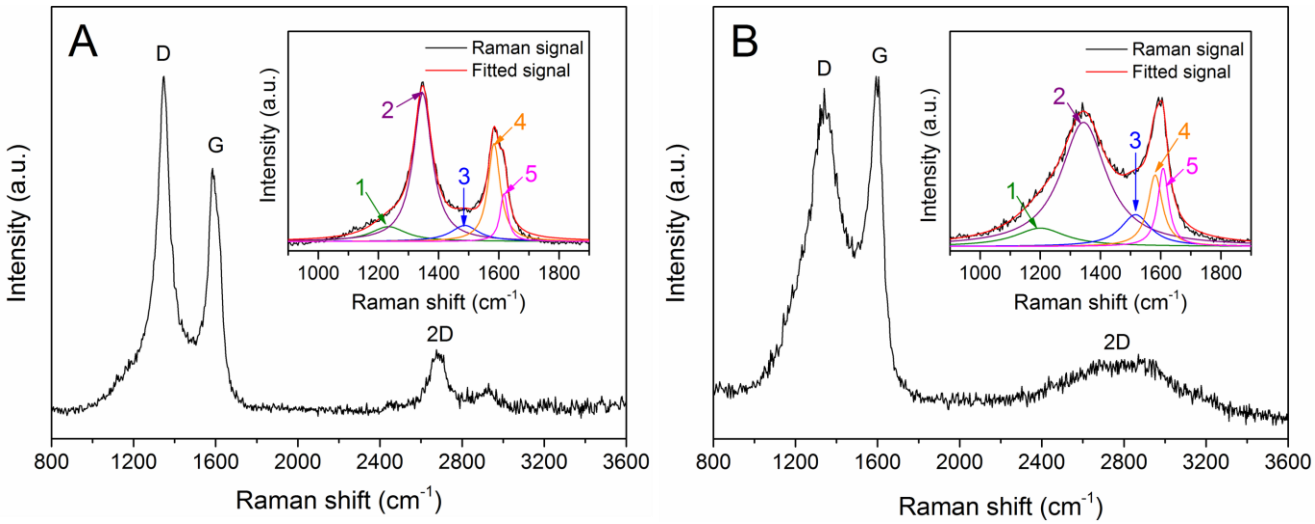

Figure 3. Raman spectra of the Co-Mn/CDC (A) and Co-Cu/CDC (B) fresh catalysts. Inset: Lorentzian fit deconvolution of the D and G bands.

Further information about the surface chemical composition of the prepared catalysts was obtained by XPS spectroscopy (**Figure 4**), and the quantitative results are is summarized in **Table 1**. **Figure 4A** shows the high resolution XPS spectra of the Co 2p, Mn 2p, C 1s and O 1s regions for the as-synthesized Co-Mn/CDC catalyst. It was observed that both the Co and Mn particles surface were mainly oxidized to CoO (531.6 eV (O 1s), 781.0 eV (Co 2p)) and MnO (530.3 eV (O 1s), 642.4 eV(Mn 2p)), and no signals related to the metallic states Co^0 and Mn^0 were identified. In **Figure 4B**, the Co-Cu/CDC catalyst exhibited both the metallic states of Co^0 (779.3 eV) and Cu^0 (933.6 eV), and their respective metal oxides CoO (531.6 eV (O 1s), 781.0 eV (Co 2p)) and CuO (532.5 eV (O 1s), 934.4 eV(Cu 2p)), which suggest that the metal nanoparticles in this catalyst possess a relative higher stability. The surface metal oxide composition for each catalyst resulted in 100%CoO-100%MnO for Co-Mn/CDC, and 87%CoO-55%CuO for Co-Cu/CDC. On the other hand, the O 1s and C 1s spectra of both catalysts showed the presence of several functional groups involving C and O atoms. An important contribution of sp^2 carbons and, to a lesser extent, of C-O bonds was identified at ca. 285 eV and ca. 286.2 eV, respectively [22]. Besides these signals, the Co-Mn/CDC catalyst exhibited two additional peaks at 285.2 eV and 290.9 eV, related to the presence of sp3 carbons and the π-π^* transition in the graphitic support, respectively [23].

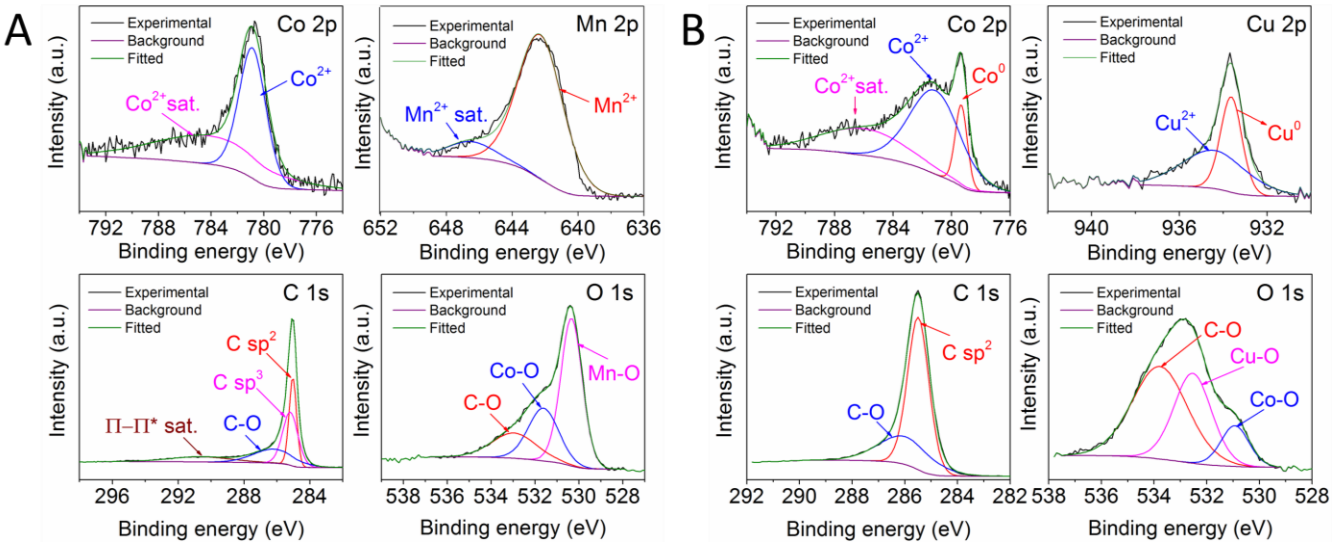

Figure 4. High resolution XPS spectra of the Co-Mn/CDC (A) and Co-Cu/CDC (B) fresh catalysts.

Table 1. Surface atomic composition of the fresh catalysts obtained by XPS spectroscopy.

Sample	Overall surface composition (at.%)					Cobalt content (at.%)		Manganese content (at.%)		Copper content (at.%)	
	O	C	Co	Mn	Cu	Co^0 (779.3 eV)	CoO (781.0 eV)	Mn^0 (638.7 eV)	MnO (642.4 eV)	Cu^0 (933.6 eV)	CuO (934.4 eV)
Co-Mn/CDC	7.0	90.5	0.9	1.6	—	0.0	100.0	0.0	100.0	---	---
Co-Cu/CDC	7.9	89.8	1.6	—	0.7	13.0	87.0	---	---	44.6	55.4

3.2. Catalytic decomposition of methane on Co-Cu/CDC catalyst

3.2.1. Influence of the reaction temperature

In order to evaluate the effect of the reaction temperature on the yield and morphology of the carbonaceous nanomaterials grown, Co-Cu/CDC catalyst was operated from 650 ºC to 975 ºC using a feed gas composition of 28.6%CH_4:14.3%H_2:57.1%N_2. **Figure 5** shows that both the productivity and carbon growth rate were favored with the increase in temperature, reaching a maximum production of 0.33 gC/gcat·h at 800 ºC. This enhancement can be due to high temperatures promote a faster diffusion rate of the carbon atoms through the metal nanoparticles, increasing the carbon precipitation and, therefore, the growth rate of the carbonaceous nanomaterials formed [12]. The evolution of carbon mass seemed to follow a linear growth from 650ºC to 750ºC with a constant rate along the reaction time evaluated. However, by increasing the temperature above 800 ºC, the carbon mass evolution reached a plateau before

120 min of reaction, which could be due to the partial deactivation of the catalyst, either by carbon encapsulation or by steric hindrance effects [9,24].

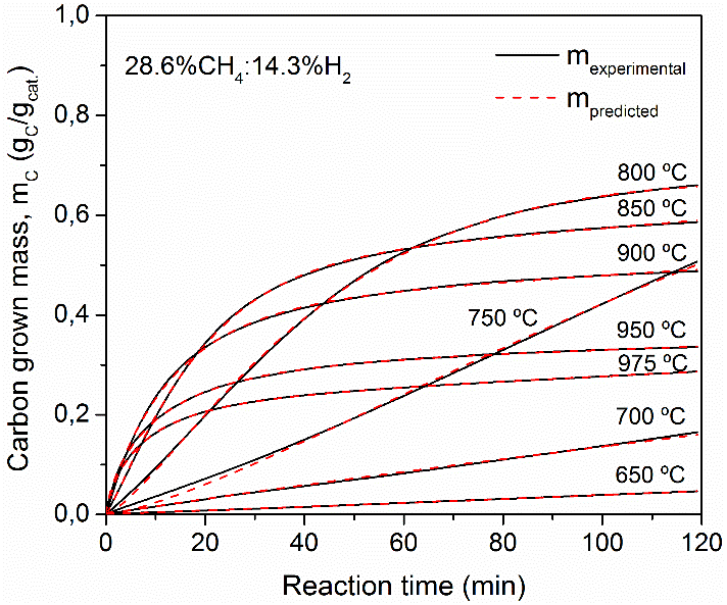

Figure 5. Influence of the reaction temperature on the carbon growth (gC/gcat.) evolution over time, using the Co-Cu/CDC catalyst with a feed composition of 28.6% CH_4:14.3% H_2:57.1% N_2.

Accordingly, the electron microscopy characterization shown in **Figure 6** indicates that the formation of carbonaceous nanomaterials over the Co-Cu/CDC catalyst underwent a transition around 850 ºC. Bellow this temperature, the catalytic methane decomposition reaction was selective towards the formation of bamboo-like carbon nanotubes. However, when the temperature was increased above, the carbonaceous material formed exhibited a graphitic-like morphology surrounding the metal nanoparticles, which explains the early catalyst deactivation and the low productivity observed in the carbon evolution curves of **Figure 5** at high reaction temperatures.

In addition, as a result of the increase in the reaction temperature, an increase in both the outer diameter and the length size of the CNTs was also evidenced. For instance, the outer diameter of the CNTs synthesized was increased from 28 nm to 59 nm when the temperature was increased from 650 ºC to 850 ºC, respectively. This result can be explained because the increase in temperature promotes the sintering of metal particles, which strongly influences the final dimensions of the CNTs. Consequently, a larger reconstruction and sintering of the metal nanoparticles were observed with the raising of the reaction temperature.

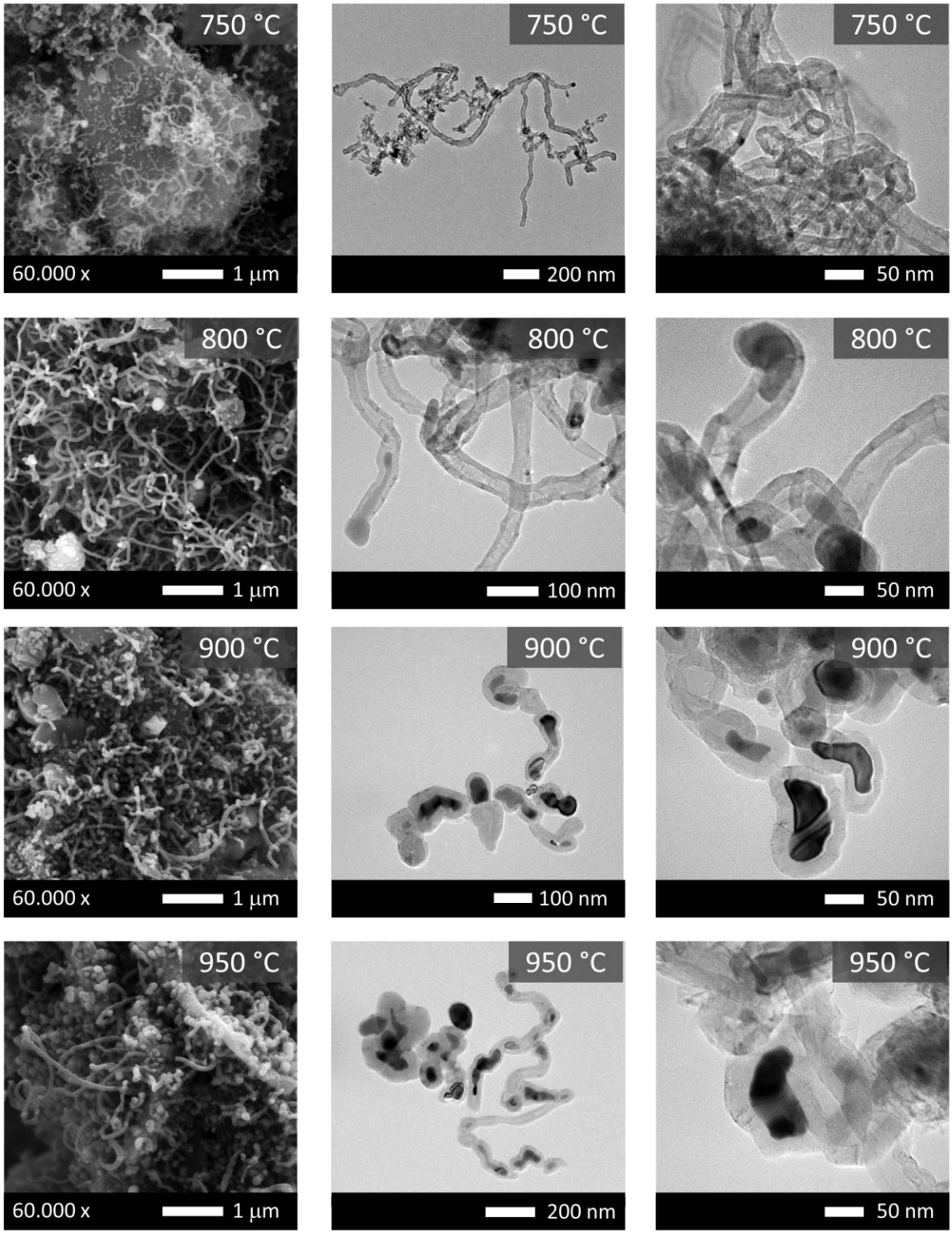

Figure 6. SEM and TEM images of the carbonaceous nanomaterials obtained with the Co-Cu/CDC catalyst using a feed composition of 28.6% CH_4:14.3% H_2:57.1% N_2 at different reaction temperatures.

Table 2 summarizes the textural properties of the Co-Cu/CDC catalyst before and after reaction at different temperatures using a feed composition of 28.6% CH_4:14.3% H_2:57.1% N_2. The fresh Co-Cu/CDC catalyst exhibited a surface area of 438 m^2/g, 0.194 cm^3/g pore volume, 87% microporosity and an average pore diameter of 0.77 nm. After the catalytic methane decomposition, both the surface area and the porosity of the catalyst was reduced as the reaction temperature was increased which can be due to the blockage of pores by the carbonaceous nanomaterials grown. This result confirms the enhancement of the production yield with the temperature increment, which agrees with the carbon evolution curves of **Figure 5** and the micrographs shown in **Figure 6**.

Table 2. Textural properties of the Co-Cu/CDC catalyst before and after CDM reaction at different temperatures using a feed composition of 28.6% CH_4:14.3% H_2:57.1% N_2.

Sample	BET surface (m^2/g)	Pore volume* (cm^3/g)	Micropore volume** (cm^3/g)	Micropore volume (%)
Co-Cu/CDC fresh catalyst	438	0,206	0.160	78
700°C	388	0.244	0.144	59
750°C	204	0.184	0.066	36
800°C	69	0.168	0.023	14

*Total pore volume at P/Po> 0.989, **Estimated from the t-plot method

3.2.2. Influence of the feed gas composition

Due to the high selectivity of the Co-Cu/CDC catalyst towards the formation of carbon nanotubes at relative low temperatures (below 850 ºC), a study of the influence of the feed gas composition on the productivity of the CNTs was performed varying the CH_4 and H_2 concentration from 7.1% to 42.9% (**Figure 7**). All the experiments were conducted at 750 ºC due to the high carbon productivity and low deactivation of the Co-Cu/CDC catalyst observed during the CDM reactions at different temperatures. **Figure 7A** shows that the increase in the partial pressure of CH_4 enhances both the productivity and growth rate of CNTs. This is because during the CDM reaction, the increase in the CH_4 concentration promotes the carburization of the metal nanoparticles, increasing the number of carbon atoms dissolved in them, and therefore the precipitated carbon amount at the metal-support interface is greater [25]. In this case, a maximum productivity of 0.38 gC/gcat·h was reached using a feed composition of 42.9%CH_4:14.3%H_2:42.9%N_2.

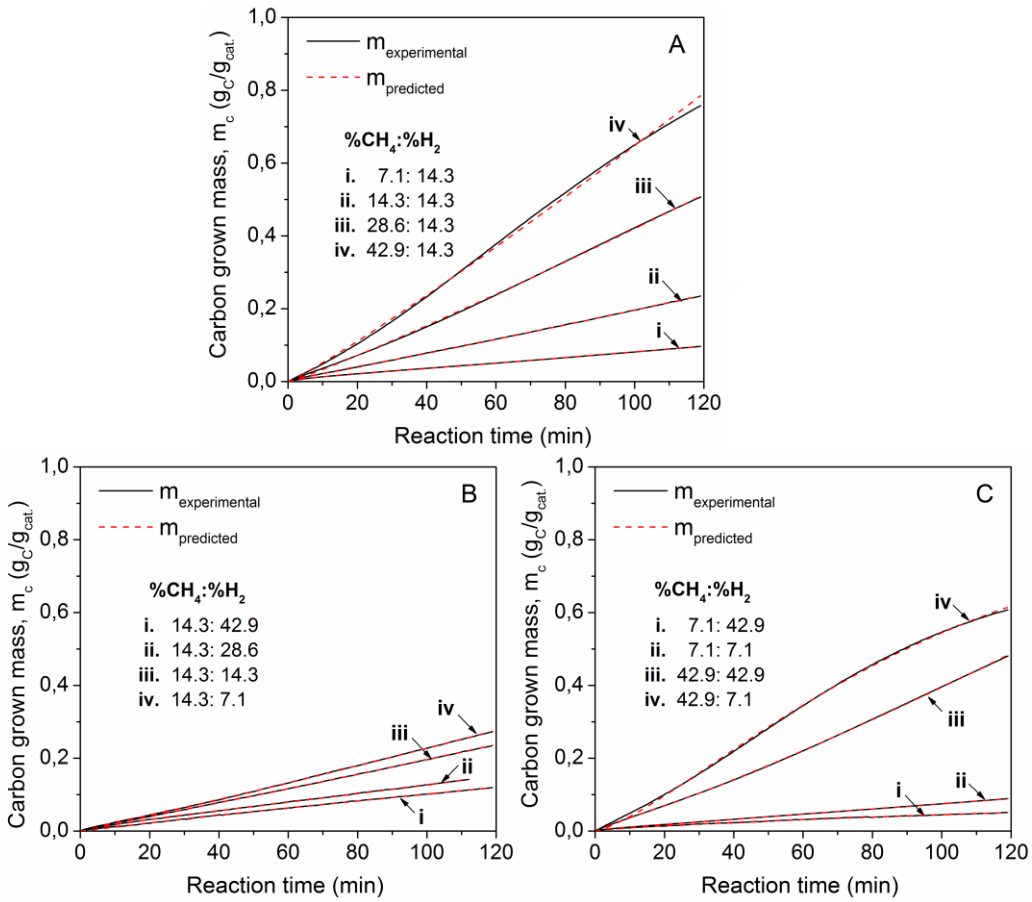

Figure 7. Influence of the feed gas composition on the carbon growth (gC/gcat.) evolution over time, operating the Co-Cu/CDC catalyst at 750 ºC. Effect of the partial pressure of methane (A), partial pressure of hydrogen (B) and extreme feed gas compositions (C).

Conversely, it was observed that the increase of the H_2 concentration resulted in low carbon productivity and a low CNTs growth rate (**Figure 7B**). This can be due to the CH_4 adsorption sites on the metal nanoparticles surface are occupied by H_2 molecules in excess, which hinders the catalytic decomposition of methane and the initial stage of the carburization process [25]. This fact was evident when an extreme concentration of CH_4 and H_2 was used in the feed gas mixture (**Figure 7C**).

The electron microscopy images in **Figure 8** revealed that a high CH_4 concentration shortened the length of the CNTs synthesized, which indicates the early deactivation of the metal nanoparticles by the accumulation of amorphous carbon coating their surface. This coke coating hampers the formation of the metallic carbide and, therefore, the diffusion of more carbon atoms through the nanoparticles is limited, leading to a premature growth termination [24].

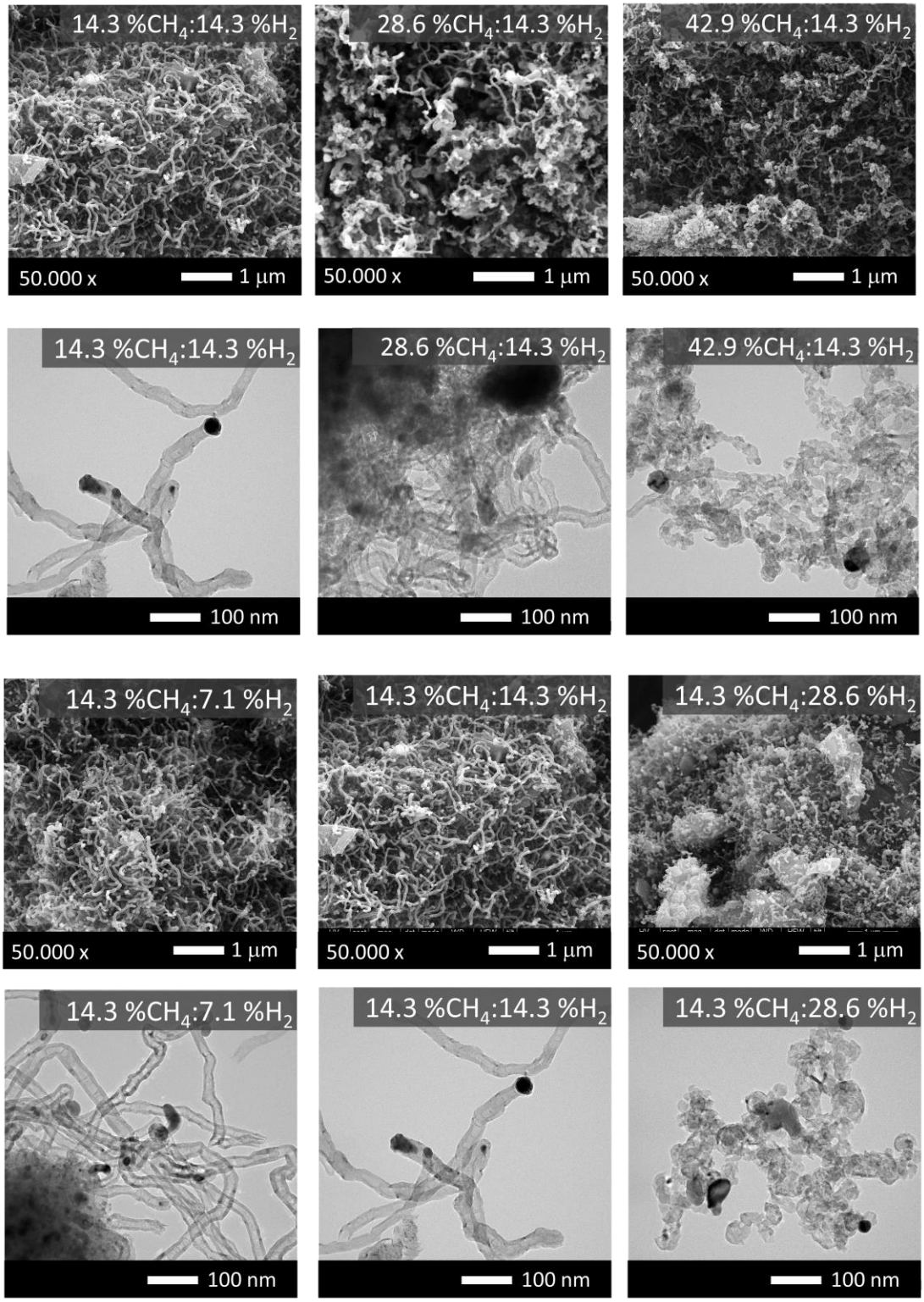

Figure 8. Influence of the feed gas composition on the morphology of the carbon nanotubes obtained with the Co-Cu/CDC catalyst operated at 750 ºC.

3.2.3. Influence of the operation conditions on the CNMs quality

The influence of the operation conditions —reaction temperature and feed gas composition— on the quality of the CNMs obtained was characterized by the I_G/I_D and I_{2D}/I_G ratio from the Raman spectra shown in **Figure 9**. In all samples, the three characteristic peaks corresponding to the D band (1350 cm^{-1}), the G band (1590 cm^{-1}), and the 2D band (2700 cm^{-1}) were identified. As was mentioned before, the I_G/I_D ratio between the G band (1590 cm^{-1}, assigned to the in-plane vibration of the sp^2 bonds) and the D band (~1350 cm^{-1}, typical of defective graphite-like materials) was used as a quantitative measure of the structural disorder degree in the carbonaceous materials. On the other hand, the I_{2D}/I_G ratio is strongly correlated to the number of layers in the graphene-like materials [26]. In a monolayer graphene, this ratio is usually $I_{2D}/I_G > 2$, while for bi-layer graphene film the ratio is $1<I_{2D}/I_G<2$ and, in the case of the multilayer graphene, it is $I_{2D}/I_G < 1$ [27]. From **Figure 9A**, it was observed that the increase in the reaction temperature enhanced the quality of the CNTs reaching a maximum $I_G/I_D=2.31$ at 850 ºC using a feed gas composition of 28.6%CH_4:14.3%H_2:57.1%N_2. In addition, as the temperature increases, the separation between the bands D and G became larger, and the intermediate peak between both bands almost disappeared. This is indicative of the surface coverage degree of the support by the carbon formed, which was evidently larger as the productivity increased [25]. From 800 ºC, the intensity of the 2D band became higher, which suggest a transition in the obtained carbonaceous nanomaterials towards the formation of a graphitic/graphenic carbon structure. The intensity ratio $I_{2D}/I_G<0.50$ indicates that such new carbon structures formed are graphitic in nature with more than 5 graphene layers [28].

Regarding the variation of the feed composition (**Figure 9B**), it was observed that the increase in the CH_4 concentration decreased the I_G/I_D ratio of the CNTs obtained and, in this case, the maximum quality $I_G/I_D=1.08$ was reached by using a composition of 14.3%CH_4:14.3%H_2:71.4%N_2. As mentioned before, a high CH_4 concentration shortens the CNTs and promotes the formation of amorphous carbon that accumulates on both the top and the bottom of the nanotube. Therefore, as the nanotubes become smaller, the density of defects due to such amorphous carbon accumulation becomes greater [29]. However, the clearer separation between the bands D and G as the raising of the methane concentration indicates that the productivity of the carbonaceous nanomaterials was increased. On the other hand, in **Figure 9C** it was found that the increase in the hydrogen concentration improved the quality of the carbonaceous nanomaterials due to the ability of H_2 to gasify part of the amorphous carbon formed on the metal

nanoparticles surface [25]. The maximum quality I_G/I_D=1.08 was also reached by using a moderated feed gas composition of 14.3%CH_4:14.3%H_2:71.4%N_2.

Consequently, these results demonstrate the importance of finding the most suitable feed gas composition that balances both the productivity and the quality of the CNMs formed.

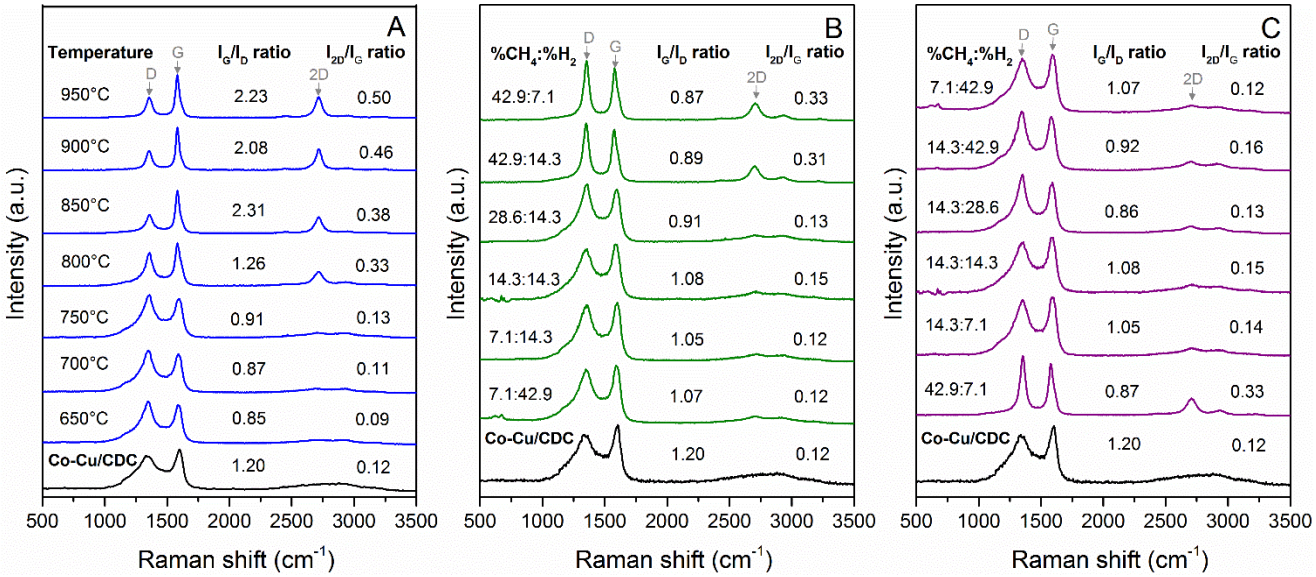

Figure 9. Raman spectra of the carbonaceous nanomaterials synthesized at different operation conditions: effect of the reaction temperature (A), and effect of the feed gas composition varying the partial pressure of methane (B) and the partial pressure of hydrogen (C).

3.3. Catalytic decomposition of methane on Co-Mn/CDC catalyst

3.3.1. Influence of the reaction temperature

Figure 10 shows the effect of the reaction temperature on the carbon mass evolution over time, using the Co-Mn/CDC catalyst with a feed composition of 28.6%CH_4:14.3%H_2:57.1%N_2. The shape of the carbon evolution curves exhibits a high initial slope corresponding to a high starting reaction rate, which gradually decreases until attaining a certain g_C/g_{cat}. value, indicating a reduction in the growth rate of the CNMs formed. The rate attained at the final operation time is determined by the residual activity of the catalyst, in which the H_2 generated in situ during the reaction, gasifies a fraction of the amorphous carbon formed on the metal surface, thereby exposing some active centers responsible for the stationary activity [10]. It was observed that both the productivity and growth rate of CNMs were favored with the increase in temperature, reaching a maximum of 0.48 gC/gcat·h at 975 ºC. A transition in the carbon mass evolution

curves was also identified about 850 ºC, suggesting a change in the balance between the carbon nucleation and precipitation steps during the CNMs formation [12]. Below this temperature, the carbon growth rate followed a quasi-linear slope along the reaction time. However, at higher temperatures, the growth rate starts to decelerate after 20 min of reaction, which can be due to the partial deactivation of the catalyst, as was explained before.

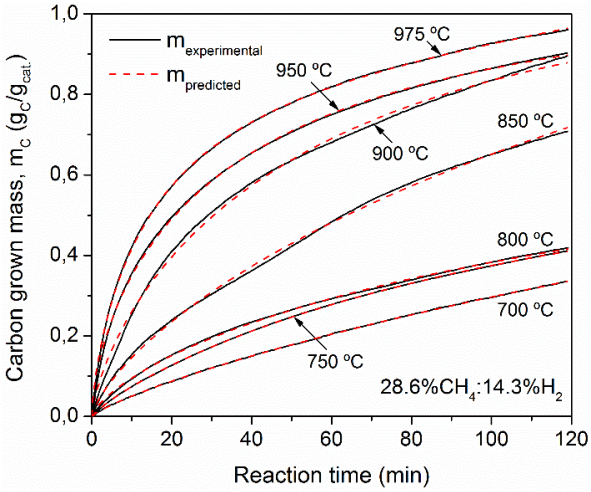

Figure 10. Influence of the reaction temperature on the carbon growth (gC/gcat.) evolution over time, using the Co-Mn/CDC catalyst with a feed composition of 28.6% CH_4:14.3% H_2:57.1% N_2.

In line with the productivity enhancement observed in the CDM experiments at high temperatures, the textural properties of the fresh Co-Mn/CDC catalyst were decreased after reaction, which can be due to the blockage of pores by the carbonaceous nanomaterials grown, **Table 3**. In fact, the micropores of the fresh catalyst were strongly affected, so that the micropore volume could not be estimated because the calculated external surface area was larger than the total BET surface area.

Table 3. Textural properties of the Co-Mn/CDC catalyst before and after CDM reaction at different temperatures using a feed composition of 28.6% CH_4:14.3% H_2:57.1% N_2.

Sample	BET surface (m^2/g)	Pore volume* (cm^3/g)	Micropore volume** (cm^3/g)	Micropore volume (%)
Co-Mn/CDC fresh catalyst	64	0.120	0.031	26
850°C	58	0.167	---	0
900°C	40	0.131	---	0
950°C	20	0.084	---	0

*Total pore volume at P/Po> 0.989, **Estimated from the t-plot method

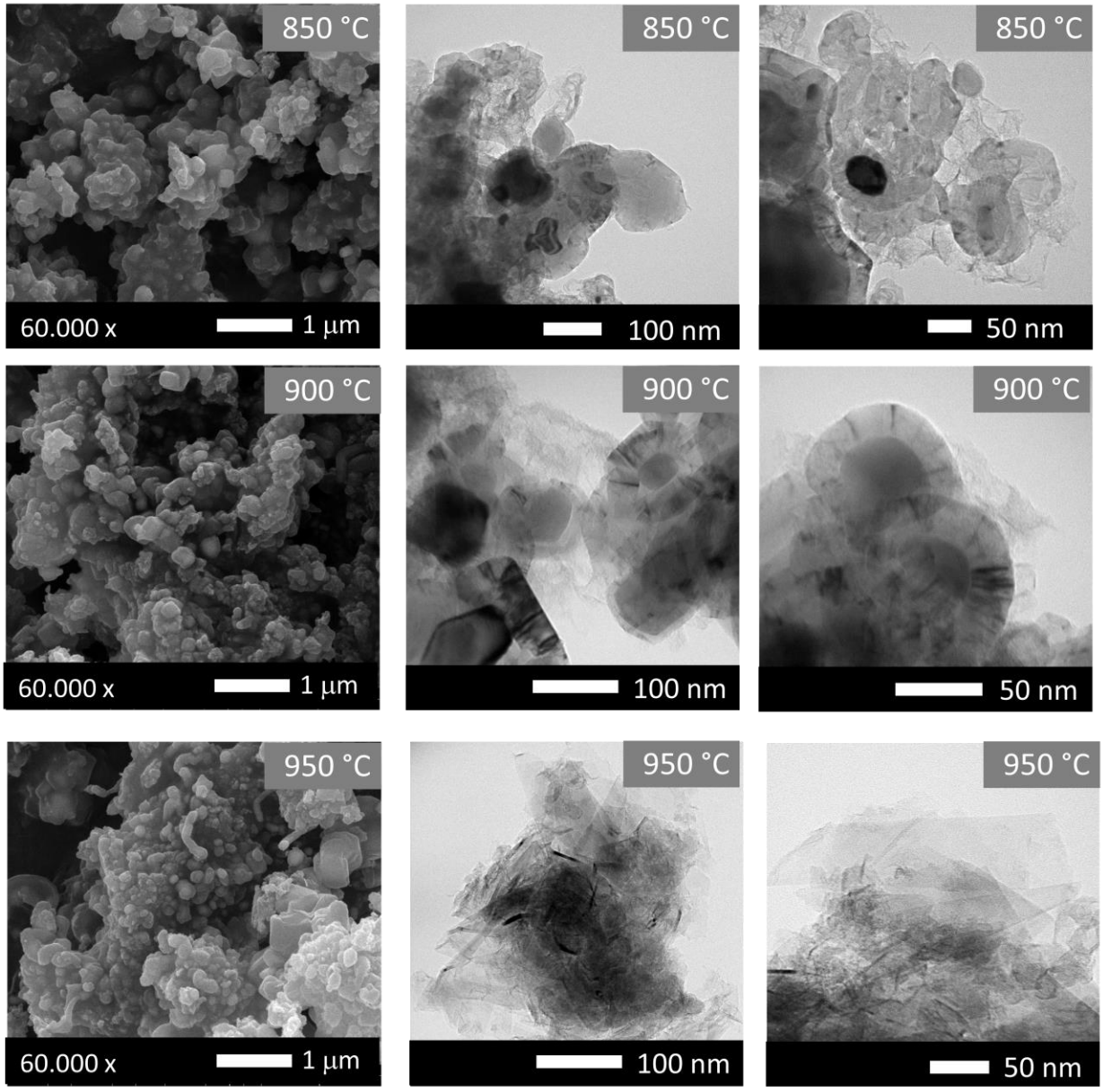

Figure 11. SEM and TEM images of the carbonaceous nanomaterials obtained with the Co-Mn/CDC catalyst using a feed composition of 28.6% CH_4:14.3% H_2:57.1% N_2 at different reaction temperatures.

Electron microscopy characterization in **Figure 11** shows that the surface of the Co-Mn/CDC catalyst became smoother after the CDM reaction and the formation of carbon nanotubes was not detected along the temperature range evaluated. Unlike the Co-Cu/CDC catalyst, a mixture of few-layer graphene (FLG), graphite nanolayers and graphene nanoflakes surrounding the metal nanoparticles was observed using the Co-Mn/CDC as catalyst in the CDM reaction. The modification of the Co/CDC catalyst with Mn allowed

directing the selectivity towards the production of layered graphene nanomaterials, which can be attributed to the synergic effect of its bigger particle size and higher carbon solubility comparing with the Cu nanoparticles. It has been observed that metals with high carbon solubility, such as Ni, can dissolve a large quantity of carbon in the bulk and therefore can precipitate more substantial amounts of carbon atoms on the metal surface, which upon cooling from high growth temperatures, favors the formation of graphitic and/or multilayered graphenic materials [30]. On the other hand, the large size of the Mn particles can provide a higher number of nucleation sites available for the growth of two-dimensional CNMs comparing with the small size of the Cu nanoparticles, in which the growth of one-dimensional materials is preferred.

According to previous works developed by the CREG research group [8-12], both the type of carbonaceous nanomaterial formed, and their rate of growth are consequence of a subtle equilibrium between the nucleation and segregation-precipitation rates at the exit points of the metal nanoparticles. If the nucleation rate is low, the formation of CNTs and CNFs is favored because, once the precipitation of the carbon atoms begins, the carbon concentration inside the nanoparticle is undersaturated, and the growth of one-dimensional materials is observed (**Figures 6** and **8**). On the contrary, if the rate of nucleation is high, the number of exit points can be very large, and the precipitation of the carbon atoms occurs in parallel around the entire external surface of the metal nanoparticles, resulting in surrounding graphenic layers (**Figures 11** and **13**).

3.3.2. Influence of the feed gas composition

The effect of the gas composition on the yield and morphology of the CNMs grown with the Co-Mn/CDC catalyst was further evaluated at 950 ºC varying the CH_4 and H_2 concentration from 7.1% to 28.6%, **Figure 12**. Similar to the Co-Cu/CDC catalyst, the increase in the partial pressure of CH_4 enhanced both the productivity and growth rate of the CNMs obtained (**Figure 12A**). In this case, the maximum productivity reached was 0.47 gC/gcat·h using a feed composition of 28.6%CH_4:28.6%H_2:42.9%N_2. This fact can be explained because during CDM reaction, the high CH_4 concentrations improve both the catalytic decomposition rate of methane and the metal particle carburization. At high reaction temperatures, the amount of the carbon atoms dissolved becomes higher and consequently, the driving force for their diffusion through the metal nanoparticles increases, which promotes a high precipitation rate to form the carbonaceous nanomaterials [31].

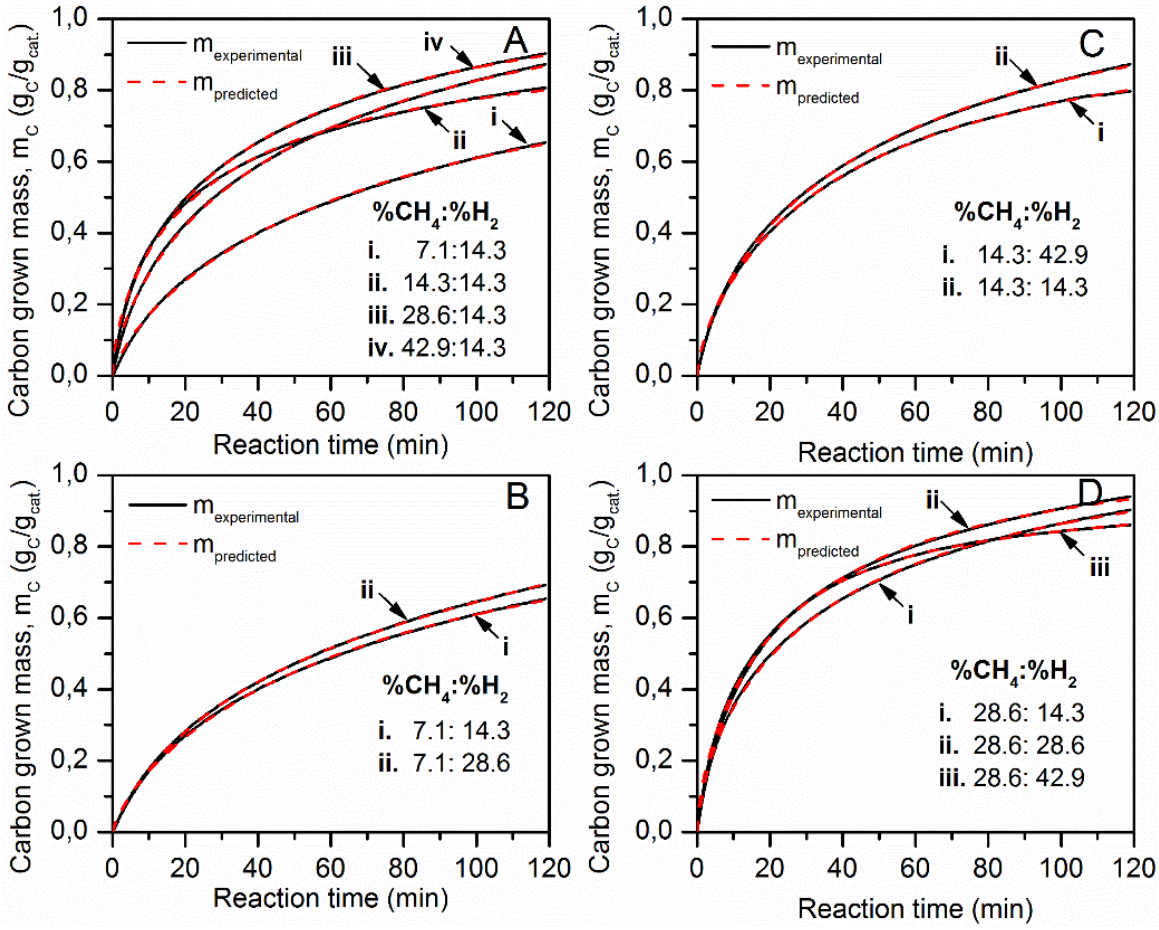

Figure 12. Influence of the feed gas composition on the carbon growth (gC/gcat.) evolution over time, operating the Co-Mn/CDC catalyst at 950 ºC. Effect of the partial pressure of methane (A) and partial pressure of hydrogen with different CH_4/H_2 ratios (B, C and D).

Electron microscopy images in **Figure 13** show the growth of unstructured carbon layers and graphite platelets surrounding the metallic nanoparticles, which by the action of the reaction atmosphere, mainly hydrogen, can evolve to form FLG materials [25]. It was observed that the increase in CH_4 concentration extends the lateral size of the obtained graphenic nanomaterials, and some isolated graphene nanoflakes of around 200 nm could be observed using a moderated feed gas composition of 14.3%CH_4: 14.3%H_2:71.4%N_2.

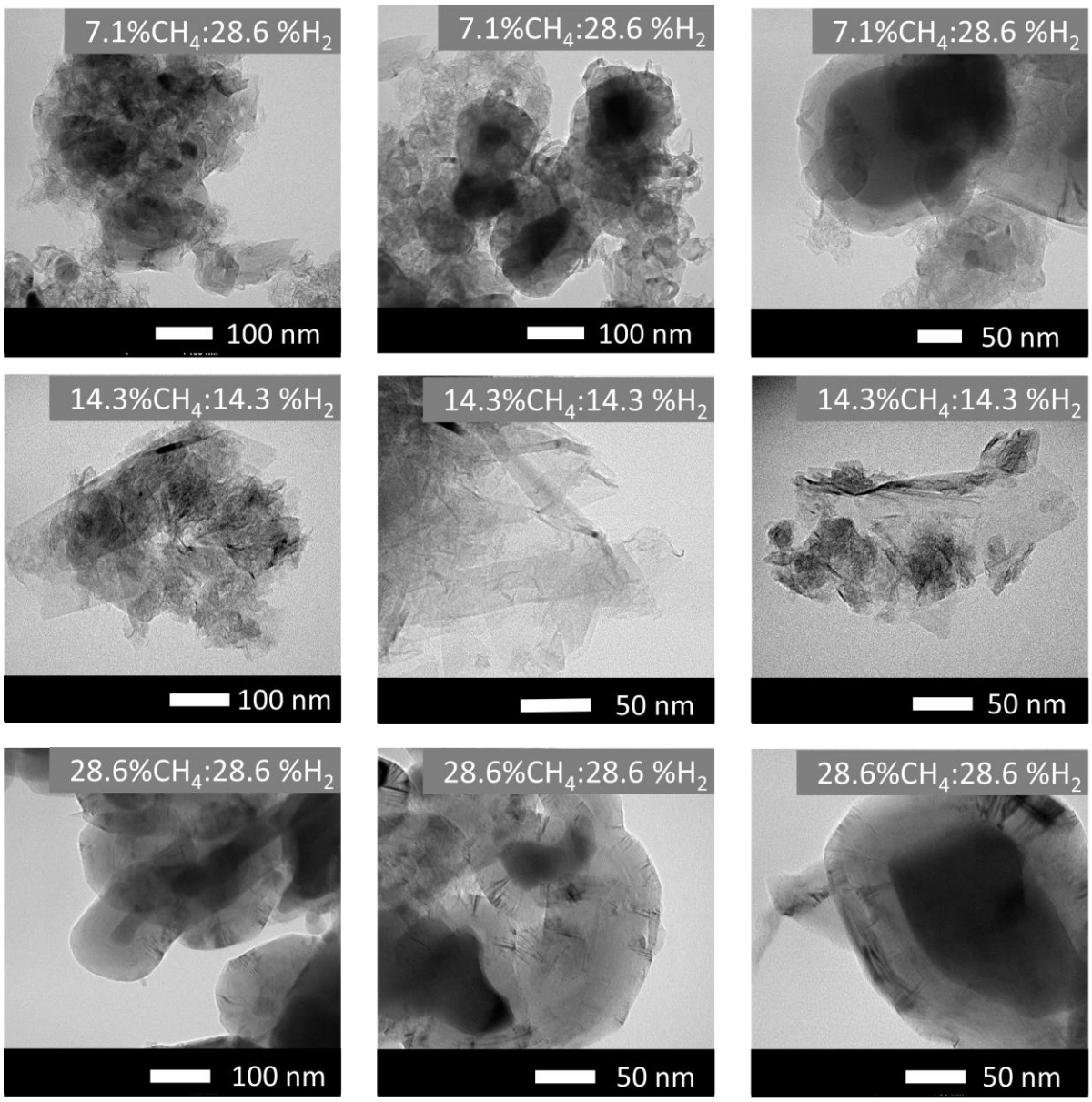

Figure 13. Influence of the feed gas composition on the morphology of the carbonaceous nanomaterials obtained with the Co-Mn/CDC catalyst operated at 750 ºC.

3.3.3. Influence of the operation conditions on the CNMs quality

The quality of the carbonaceous nanomaterials obtained at different reaction conditions was characterized by the I_G/I_D and I_{2D}/I_G ratios from the Raman spectra shown in **Figure 14**. Besides the D and G bands centered at 1350 cm^{-1} and 1590 cm^{-1}, respectively, the characteristic 2D band (2700 cm^{-1}) was detected in all the spectra confirming the formation of graphenic carbonaceous nanomaterials [32].

From **Figure 14A** it was observed that the I_{2D}/I_G ratio was enhanced by increasing the reaction temperature, which suggests a reduction in the layers staked in the carbonaceous nanomaterials obtained. Thus, the I_{2D}/I_G ratio varied from 0.33−0.45 between 700 ºC and 850 ºC characteristic of graphitic materials with more than 5 layers, to 0.55−0.64 between 900 ºC and 975 ºC, attributed to the formation of FLG materials with 4 layers of graphene [28]. However, it was also observed that high reaction temperatures increased the degree of structural defects I_G/I_D. Therefore, although, the amount of carbon formed increases at high reaction temperatures (**Figure 10**), the average quality of the carbonaceous nanomaterials obtained is lower. Considering both I_G/I_D and I_{2D}/I_G ratios, the maximum quality achieved varying the reaction temperature was I_G/I_D= 2.50 and I_{2D}/I_G=0.64 at 900 ºC.

Regarding the variation of CH_4 and H_2 in the feed composition (**Figure 14B**), keeping a constant temperature of 950 ºC, it was observed that the increase in the CH_4 concentration promoted the increase of the I_{2D}/I_G ratio and, in this case, the maximum quality I_{2D}/I_G=0.80 and I_G/I_D=2.62 was reached by using a composition of 28.6%CH_4:28.6%H_2:42.8%N_2. The intensity ratio I_{2D}/I_G=0.80 indicates that, under this reaction conditions, it was possible to obtain a FLG carbonaceous material with at least 3 layers of graphene [28].

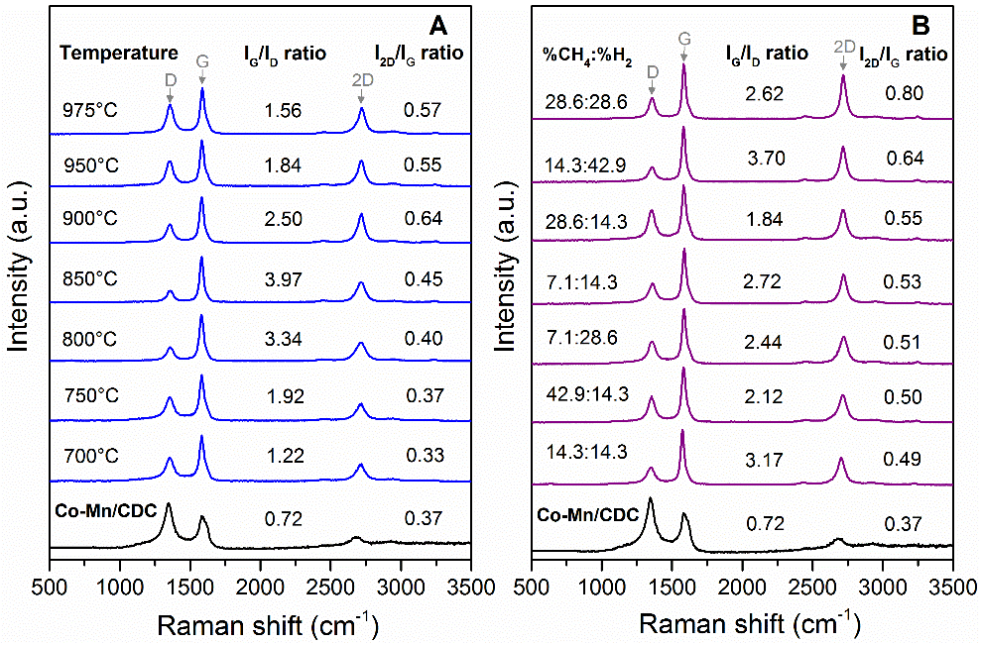

Figure 14. Raman spectra of the carbonaceous nanomaterials synthesized with Co-Mn/CDC at different operation conditions: effect of the reaction temperature (A), and effect of the feed gas composition (B).

4. Conclusions

The incorporation of Cu or Mn on the Co/CDC catalysts allowed the selective production of carbon nanotubes below 850 ºC (Co-Cu/CDC) and graphene-related nanomaterials above 900 ºC (Co-Mn/CDC) during the catalytic decomposition of methane.

The difference in the selectivity of the catalysts towards the formation of a specific carbonaceous nanomaterial might be due to the combined effect of the metal particle size and its carbon solubility. Manganese, which has a higher carbon solubility and presented a bigger particle size than copper, can favor the formation of two-dimensional CNMs, because can dissolve a larger quantity of carbon in the bulk and, therefore, can precipitate more substantial amounts of carbon atoms on the metal surface. Additionally, the large size of the Mn particles might provide a higher number of nucleation sites available for the carbon growth and consequently, the precipitation of the carbon atoms can occur in parallel around the entire external surface of the metal nanoparticles, resulting in surrounding graphenic layers. On the other hand, due to the low carbon solubility and the small size of the copper nanoparticles in the Co-Cu/CDC catalyst, the precipitation rate of the carbon atoms on the metal surface is higher than the carbon nucleation rate and therefore the formation of CNTs and CNFs is favored.

Regarding the variation of the operating conditions during the CDM reaction, it was found that the productivity and carbon growth rate in both catalysts increased with temperature and the CH_4 concentration in the feed. This is because during the CDM reaction, the increase in the CH_4 concentration promotes the carburization of the metal nanoparticles, increasing the number of carbon atoms dissolved in them, and therefore the precipitated carbon amount at the metal-support interface is greater. The maximum productivity reached by the Co-Mn/CDC catalyst was 0.48 gC/gcat·h at 975 °C with a feed composition of 28.6%CH_4:14.3%H_2:57.1%N_2. On the other hand, in the Co-Cu/CDC catalyst this productivity was 0.38 gC/gcat·h at 750 °C using a feed composition of 42.9%CH_4:14.3%H_2:42.9%N_2.

The quality of the CNMs synthesized, measured by the I_G/I_D and I_{2D}/I_G ratios from the Raman spectra, was highly sensitive to the operating conditions used in the CDM reaction. In the case of CNTs production, the I_G/I_D ratio was enhanced by using high temperatures and low CH_4 concentrations. The maximum quality I_G/I_D=2.31 was attained at 850 ºC using a feed gas composition of 28.6%CH_4:14.3%H_2:57.1%N_2. On the other hand, the I_{2D}/I_G ratio of the graphene-related nanomaterials was improved by increasing both the temperature and the CH_4 concentration in the feed. Considering both I_G/I_D and I_{2D}/I_G ratios, the

maximum quality achieved by the Co-Mn/CDC catalyst was I_{2D}/I_G=0.80 and I_G/I_D=2.62 using a composition of 28.6%CH_4:28.6%H_2:42.8%N_2 at 950 ºC. The intensity ratio I_{2D}/I_G=0.80 indicates that, under this reaction conditions, it was possible to obtain a FLG carbonaceous material with at least 3 layers of graphene.

5. Acknowledgements

I would like to express my most sincere gratitude to Dr. Antonio Monzón and Dr. Eva Romero for giving me the opportunity to work in their group, and especially to Dr. Fernando Cazaña for his valuable guidance and immense accompaniment during the entire development of this work. I could not have had a better mentor for the experiments and data interpretation. The financial support from the Project ENE2017-82451-C3 (MINECO-FEDER, Madrid- Spain) and the scholarship sponsored by Fundación Carolina (Madrid, Spain) and the University of Zaragoza is gratefully acknowledged. Personally, I would like to thank my classmates for the great friendship that we have built in the last months. And, most importantly, thank you to my family and to all those professors & friends from Colombia for the encouragement from the distance, because without their help I could not be here making this dream come true.

6. References

[1] Liu, W. W., Chai, S. P., Mohamed, A. R., & Hashim, U. (2014). *Journal of Industrial and Engineering Chemistry*, 20(4), 1171-1185.

[2] Kumar, M., & Ando, Y. (2010). Journal of nanoscience and nanotechnology, 10(6), 3739-3758.

[3] Brukh, R., & Mitra, S. (2006). Chemical physics letters, 424(1-3), 126-132.

[4] Aguiar-Hualde, J. M., Magnin, Y., Amara, H., & Bichara, C. (2017). Carbon, 120, 226-232.

[5] Rümmeli, M. H., Bachmatiuk, A., Börrnert, F., Schäffel, F., Ibrahim, I., Cendrowski, K., ... & Büchner, B. (2011). Nanoscale research letters, 6(1), 303.

[6] Cazana, F., Galetti, A., Meyer, C., Sebastián, V., Centeno, M. A., Romeo, E., & Monzon, A. (2018). Catalysis Today, 301, 226-238.

[7] Park, J. G., Basnet, B., Kim, S. Y., Kim, S. Y., & Kim, I. J. (2017). Journal of Ceramic Processing Research, 18(8), 575-579.

[8] Rodríguez, J. C., Peña, J. A., Monzón, A., Hughes, R., and Li, K. (1995). Chem. Eng. J. 58, 7–13.

[9] Monzón, A., Lolli, G., Cosma, S., Mohamed, S. B., and Resasco, D. E. (2008). J. Nanosci. Nanotechnol. 8, 6141–6152.

[10] Monzón, A., Romeo, E., and Borgna, A. (2003). Chem. Eng. J. 94, 19–28.

[11] Latorre, N., Romeo, E., Cazaña, F., Ubieto, T., Royo, C., Villacampa, J. I., et al. (2010). J. Phys. Chem. C 114, 4773–4782.

[12] Azuara, M., Latorre, N., Villacampa, J., Sebastian, V., Cazaña, F., Romeo, E., & Monzón, A. (2019). Frontiers in Energy Research, 7, 34.

[13] N. Latorre, Doctoral Thesis, Escuela Politécnica Superior de Huesca, University of Zaragoza, España, 2006.

[14] Cançado, L. G., Jorio, A., Ferreira, E. M., Stavale, F., Achete, C. A., Capaz, R. B., ... & Ferrari, A. C. (2011). Nano letters, 11(8), 3190-3196.

[15] Malard, L. M., Pimenta, M. A. A., Dresselhaus, G., & Dresselhaus, M. S. (2009). Physics Reports, 473(5-6), 51-87.

[16] Ribeiro-Soares, J., Oliveros, M. E., Garin, C., David, M. V., Martins, L. G. P., Almeida, C. A., ... & Malachias, A. (2015). Carbon, 95, 646-652.

[17] Ferrari, A. C., & Robertson, J. (2001). Physical Review B, 63(12), 121405.

[18] Ferrari, A. C., & Robertson, J. (2000). Physical review B, 61(20), 14095.

[19] Dresselhaus, M. S., Jorio, A., Hofmann, M., Dresselhaus, G., & Saito, R. (2010). Nano letters, 10(3), 751-758.

[20] Lespade, P., Al-Jishi, R., & Dresselhaus, M. S. (1982). Carbon, 20(5), 427-431.

[21] McCulloch, D. G., Prawer, S., & Hoffman, A. (1994). Physical Review B, 50(9), 5905.

[22] Gong, P., Hou, K., Ye, X., Ma, L., Wang, J., & Yang, S. (2015). Materials Letters, 143, 112-115.

[23] Permatasari, F. A., Aimon, A. H., Iskandar, F., Ogi, T., & Okuyama, K. (2016). Scientific reports, 6, 21042.

[24] Latorre, N., Romeo, E., Villacampa, J. I., Cazaña, F., Royo, C., and Monzón, A. (2010). Catal. Today 154, 217–223.

[25] Cazaña, F., Latorre, N., Tarifa, P., Labarta, J., Romeo, E., & Monzón, A. (2018). Catalysis Today, 299, 67-79.

[26] Subrahmanyam, K. S., Panchakarla, L. S., Govindaraj, A., & Rao, C. N. R. (2009). The Journal of Physical Chemistry C, 113(11), 4257-4259.

[27] Tu, Z., Liu, Z., Li, Y., Yang, F., Zhang, L., Zhao, Z., ... & Richard, P. (2014). Carbon, 73, 252-258.

[28] Calizo, I., Bejenari, I., Rahman, M., Liu, G., & Balandin, A. A. (2009). Journal of applied physics, 106(4), 043509.

[29] Zhang, S., Peng, D., Xie, H., Zheng, Q., & Zhang, Y. (2017). Nano-micro letters, 9(1), 12.

[30] Dahal, A., & Batzill, M. (2014). Nanoscale, 6(5), 2548-2562.

[31] Latorre, N., Cazaña, F., Martínez-Hansen, V., Royo, C., Romeo, E., and Monzón, A. (2011). Catal. Today 172, 143–151.

[32] Graf, D., Molitor, F., Ensslin, K., Stampfer, C., Jungen, A., Hierold, C., & Wirtz, L. (2007). Nano letters, 7(2), 238-242.

Annex I. Kinetic study on the carbonaceous nanomaterials growth

According to the kinetic growth model described in [12], the carbon growth rate is determined by the net diffusion rate of the carbon atoms along the metal nanoparticles, driven by the difference of the carbon concentration at gas-side surface, C_S, and at the rear part of the nanoparticles, C_F, initially in contact with the support, where the segregation of the carbonaceous nanomaterials takes place. It can be assumed that C_F, is very low in comparison with C_S, and therefore, the reaction rate can be defined by:

$$(r_C)_t = \left(\frac{dm_C}{dt}\right)_t = k_C \cdot (C_S - C_F) \cdot a(t) \;\cong\; k_C \cdot C_S \cdot a(t) = k_C \cdot C_{S_m} \cdot \theta_S \cdot a(t) \qquad (\mathbf{1})$$

The term k_C stands for the effective carbon transport coefficient with dimensions of time^{-1} and depends on the average size of the metallic crystallites, the metallic exposed area, and the carbon atom diffusivity on the metallic nanoparticles. The catalyst activity, a, is also included in the expression, considering the possible catalyst deactivation. In turn, C_S can be calculated as a function of the carburization degree of the metal surface, θ_S, as follows: $\theta_S = C_S/C_{S_m}$, where the term C_{S_m} is the carbon concentration at the gas-side of the metal nanoparticles at complete carburization. Assuming that the carburization is a first order process [11], the evolution of the carburization with time is given by:

$$r_S = \frac{d\theta_S}{dt} = \psi_S \cdot (1 - \theta_S) \;\leftrightarrow\; \theta_S = 1 - \exp(-\psi_S \cdot t) \qquad (\mathbf{2})$$

Considering the possible residual activity of the catalyst [10], the net deactivation rate can be described as:

$$-\frac{da}{dt} = \psi_d \cdot a - \psi_r \cdot (1 - a) \;\rightarrow\; a(t) = a_R + (1 - a_R) \cdot \exp(-\psi_G \cdot t) \qquad (\mathbf{3})$$

$$\psi_G = \psi_d + \psi_r \;;\quad a_R = \frac{\psi_r}{\psi_d + \psi_r} = \frac{\psi_r}{\psi_G}$$

The terms ψ_d and ψ_r have dimensions of time^{-1} and are kinetic parameters of deactivation and regeneration, respectively. For a given catalyst composition and activation procedure, these parameters depend on the experimental conditions, mainly temperature and feed composition, used during the reaction. The term a_R corresponds to the residual activity of the catalysts, which will be zero for the case of irreversible deactivation. After combination of **Equations 1** to **3**, the carbon growth rate is given by:

$$\frac{dm_C}{dt} = j_{C_0} \cdot \theta_S(t) \cdot a(t)$$

$$\frac{dm_C}{dt} = j_{C_0} \cdot (1 - \exp(-\psi_S \cdot t)) \cdot (a_R + (1 - a_R) \cdot \exp(-\psi_S \cdot t)) \;;\; j_{C_0} = k_C \cdot C_{S_m} \quad (\mathbf{4})$$

The term m_C is the amount of carbon accumulated over the catalysts, expressed as gC/gcat. The parameter j_{C_0} represents the intrinsic carbon growth rate for the fresh catalyst, measured in gC/gcat·min, and depends on the effective carbon diffusivity in the metal nanoparticles at the operating conditions. The term C_{S_m} depends on the carbon solubility which determines the driving force for the diffusion of the carbon atoms through the metallic nanoparticles. After integration of **Equation 4**, the evolution of carbon content along time can be expressed as:

$$m_C = j_{C_0} \cdot \left(a_R \cdot \left(t - \frac{1 - \exp(-\psi_S \cdot t)}{\psi_S} \right) + (1 - a_R) \cdot \left(\frac{1 - \exp(-\psi_G \cdot t)}{\psi_G} - \frac{1 - \exp(-\psi_{SG} \cdot t)}{\psi_{SG}} \right) \right) \quad (\mathbf{5})$$

$$\psi_{SG} = \psi_S + \psi_G$$

For the particular case of a very rapid carburization step, i.e. $\psi_S \to \infty$, it can be assumed that $\theta_S = 1$, and consequently the above equations are simplified to:

$$(r_C)_t = j_{C_0} \cdot (a_R \cdot (1 - a_R) \cdot \exp(-\psi_G \cdot t))$$

$$m_C = j_{C_0} \cdot \left(a_R \cdot t + \frac{(1 - a_R)}{\psi_G} \cdot (1 - \exp(-\psi_G \cdot t)) \right) \quad (\mathbf{6})$$

In addition to the above considerations, it has been observed that there is a critical temperature in which a change of the type of carbonaceous nanomaterial formed occurs [25]. Therefore, an extra parameter, n, was incorporated as a power-law function of the reaction time, which allows modulating the effect of the diffusion time of carbon in each range of reaction temperature.

The final expression used for fitting the experimental evolution of the carbon grown concentration, m_C, was:

$$\boldsymbol{m_C = j_{C_0} \cdot \left(a_R \cdot t^n + \frac{(1 - a_R)}{\psi_G} \cdot (1 - \exp(-\psi_G \cdot t^n)) \right)} \quad (\mathbf{7})$$

Where j_{C_0} represents the intrinsic carbon growth rate for the fresh catalyst, measured in gC/gcat·min, which depends on the effective carbon diffusivity through the metallic nanoparticles at the operating conditions. The term a_R corresponds to the residual activity of the catalyst, due to the partial regeneration of the catalyst surface by action of H_2 present in the reaction. The term ψ_G is defined as the sum $\psi_G = \psi_d + \psi_r$ of the kinetic parameters of deactivation and regeneration, respectively, and has dimensions of time^{-1}.

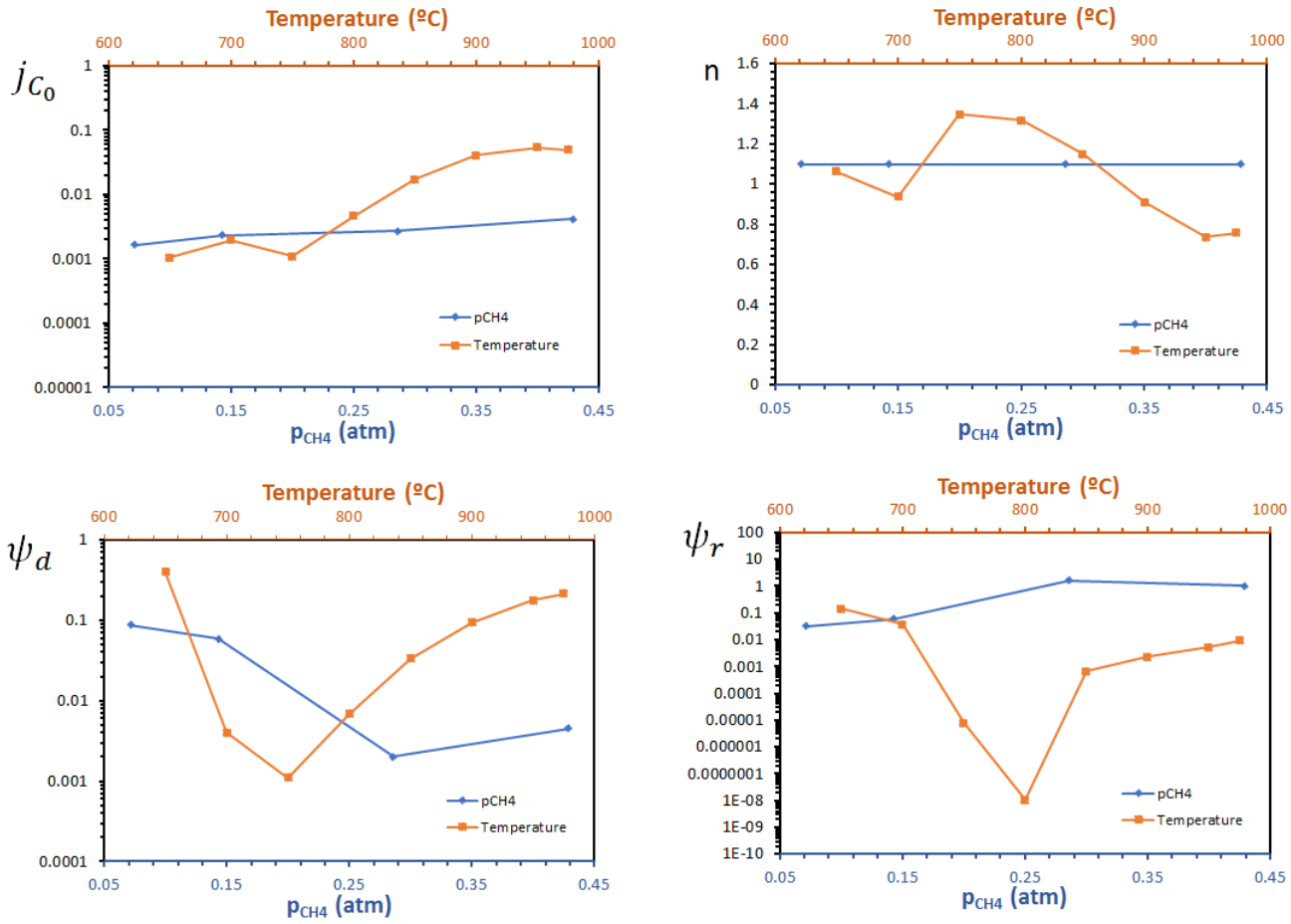

Figure S1. Influence of temperature and methane concentration on the kinetic growth parameters during the CDM reaction using the Co-Cu/CDC catalyst.

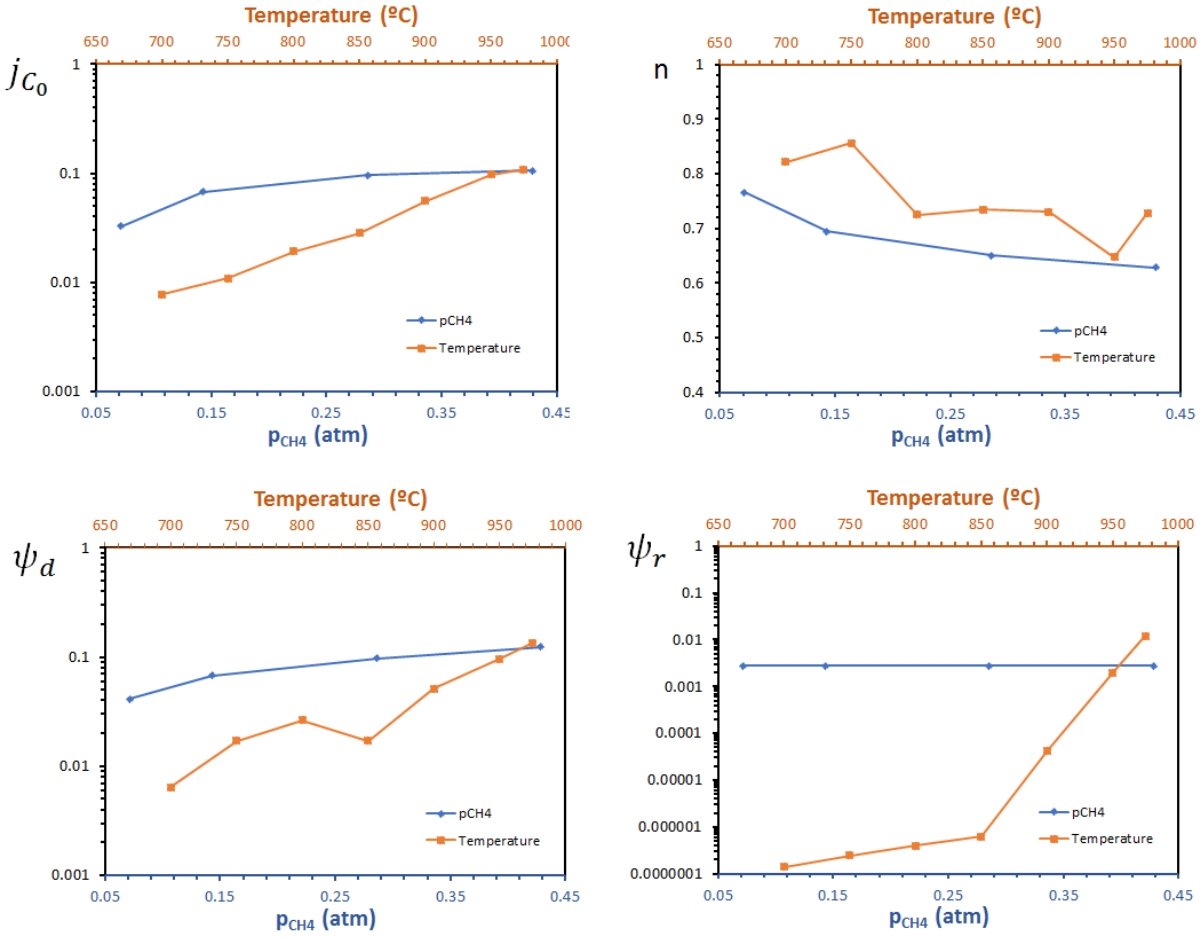

Figure S2. Influence of temperature and methane concentration on the kinetic growth parameters during the CDM reaction using the Co-Mn/CDC catalyst.